UDK 539.4:621.791.05:620.18
Original scientific article/Izvirni znanstveni članek

ISSN 1580-2949
MTAEC9, 42(1)13(2008)

ACCELERATED CREEP TESTING OF NEW CREEP RESISTING WELD METALS

PREIZKUSI POSPEŠENEGA LEZENJA ZVAROV NOVEGA JEKLA, ODPORNEGA PROTI LEZENJU

Stan T. Mandziej,[1] Anna Výrostková,[2] Mojca Šolar[3]

[1]Advanced Materials Analysis, P.O.Box 3751, 7500 DT Enschede, Nederland
[2]Institute of Materials Research SAS, Watsonova 47, 043 53 Kosice, Slovakia
[3]Elektrode Jesenice, Cesta Železarjev 8, 4270 Jesenice, Slovenia
100422.3355@compuserve.com

Prejem rokopisa – received: 2007-09-04; sprejem za objavo – accepted for publication: 2007-10-11

New creep-resisting weld metals of P91 grade were manufactured by MMA process producing multi-bead multi-layer test coupons, from which specimens were taken for accelerated creep testing on Gleeble physical simulator. The recently developed accelerated creep testing (ACT) procedure on Gleeble allows transforming in a relatively short time (less than 100 hours) the microstructure of creep-resisting materials near to the thermodynamic equilibrium state, resembling that of multi-years application at creep condition. Such advanced transformation of microstructure in the investigated weld metals after ACT was confirmed with microscopy and microanalytical study. The results also appeared to be in agreement with Thermocalc calculations. Using optimum combination of chemical compositions of the electrodes with welding procedure and post-weld heat-treatment, advantageous mechanical properties were achieved as well as results of ACT indicating potentially long creep life in exploitation conditions. In discussion of the ACT results, comparisons with results of conventional creep testing have been made. The ACT procedure appears to be useful in fast screening of newly developed creep resisting materials.

Keywords: P91 welds, accelerated creep tests, microstructure, Gleeble

Večvarkovni zvari jekla P91, odporni proti lezenju so bili pripravljeni po MMA-postopku in iz njih so bili izdelani večvarkovni vzorci za preizkuse na simulatorju Gleeble. Pred kratkim razvit preizkus pospešenega lezenja (ACT) na napravi Gleeble omogoča, da se pretvori v relativno kratkem času (manj od 100 h) mikrostruktura jekla, odpornega proti lezenju, v stanje blizu termodinamičnega ravnotežja, ki je podobno kot po mnogih letih obremenitve z lezenjem. Tako pretvorbo mikrostrukture po ACT smo potrdili z mikroskopsko in mikroanalitsko preiskavo. Zdi se, da so rezultati v skladu z izračuni na podlagi podatkov Themocalc. Z uporabo optimalne kombinacije kemične sestave elektrod, postopka varjenja in toplotne obdelavo po varjenju so bile dosežene dobre mehanske lastnosti in rezultati ACT, ki nakazujejo na potencialno dolgotrajno stabilnost pri obremenitvi z lezenjem. V razpravi primerjamo rezultate ACT z rezultati konvencionalnih preizkusov lezenja. Videti je, da je ACT-postopek koristen za hitro oceno na novo razvitih jekel, ki so odporna proti lezenju.

Ključne besede: zvari P91, poskusi pospešenega lezenja, mikrostruktura, simulator Gleeble

1 INTRODUCTION

Design of the power plant components and estimation of power plants lifetime are based on long-term creep data, which are generally available for the manufactured plate and pipe materials but seldom available for the welds on the components of the power plants. This last is mainly due to the large variety of factors appearing in the fabrication procedure, which affect the creep strength and creep life of the welds. To predict the exploitation behaviour of the welds under creep, especially of the repair welds, accelerated creep testing (ACT) procedures can be used. Such procedures of accelerated tests often apply small strains and/or constant slow deformation rates to speed-up transformation of microstructure towards that of metal alloys exploited for many years at creep conditions [6]. In general, they aim to determine in a relatively short time the remaining strength or ductility which the creep resisting materials would have after long exposure to stresses at the elevated temperatures characteristic of their exploitation.

An accelerated creep test recently developed by the Advanced Materials Analysis, Enschede, Netherlands, in collaboration with Dynamic Systems Inc, Poestenkill NY, USA [4], is a low-cycle thermal-mechanical fatigue procedure executed on Gleeble physical simulator, based on the actual knowledge of the micro- and sub-structural changes causing decay of properties during the creep. To simulate the situation of the material during creep, the following demands had to be achieved in the ACT:

- Total deformation at fracture being like at real creep – just a few percent only.
- Depletion of material's matrix in alloying elements similar to that of long-term crept steels and the carbide phases at onset of cracks being not different.
- Basic temperature and applied strains in the ACT preventing odd transformations like dissolution of carbides and/or formation of far from equilibrium phases.

These aims have been reached by considering that certain dislocations can effectively dissolve and then transport interstitial elements like C and N, and that the

annihilation of these dislocations may control the precipitation of carbides [3]. Thus accumulation of strains, generating appropriate dislocation configurations and increasing level of stored energy in the steel, was used to speed-up the transformation of microstructure. An additional factor used in the development of the ACT, known for a long time as capable of accelerating recrystallization of matrix and coagulation of carbides [1], is an electric resistance heating with controlled thermal gradients.

An initial version of this ACT procedure [4] was implemented in the "SmartWeld" EU R&D project and on purpose modified in the course of it [5]. What follows in this article is the presentation of selected ACT results and their comparison with the conventional creep-rupture tests. Further, the reliability of the ACT is confirmed by the microstructure evolution i.e. the precipitation processes and sequence of changes leading to failure, that reproduce the situations occurring in real creep. Presented here are data obtained for P91 type weld metals, manufactured in the company Elektrode Jesenice from Slovenia.

2 THE ACCELERATED CREEP TEST ON GLEEBLE – ACT

To carry out the simulative accelerated creep tests, Gleeble 3500 physical simulator was used. In this simulator in a rod-like sample made of the electrically-conductive alloy the balance between electric resistance heating of the sample and the heat flow by thermal conductivity from this sample towards the cold copper jaws allows forming a uniformly heated zone in the middle-span of the sample (see **Figure 1**). To define this zone better, on samples for the ACT a gauge portion of reduced diameter was made. Samples for the ACT were taken across multi-bead, multi-layer P91 MMA welded joints, as shown in **Figure 2**. The samples were in as-welded (marked 5s and 10s) and in post-weld heat-treated condition (marked 6s and 8s). Their chemical compositions are given in **Table 1**.

Most of the ACT samples were tested till fracture occurred, however some of them especially those for fine fractographic observations and microanalytical investigations were stopped before fracturing. As the tests for different materials were run at different temperatures, the need occurred to compare the ACT results obtained at various temperatures, to the duration of the test and its temperature had to be included in the following parameter:

$$P_{ACT} = (7 + \lg t) \cdot T/100$$

where: t = time of test in ks, and T = temperature in K.

Then, the creep strength factor in ACT has been calculated as

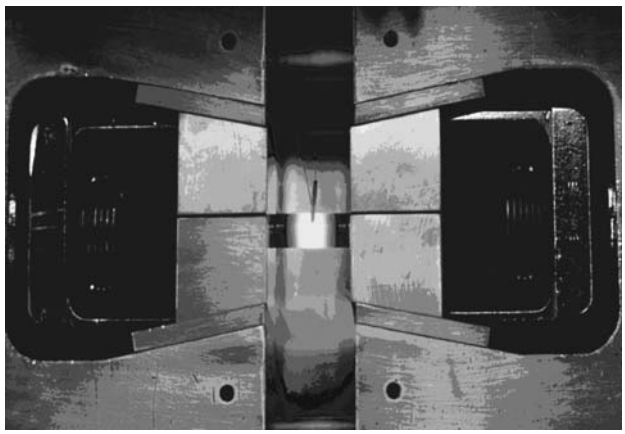

Figure 1: Example of a uniformly heated zone formed in Gleeble at the mid-span of the rod-like specimen (at temperature much higher than used in the ACT)

Slika 1: Primer enakomerno ogrete cone na napravi Gleeble na polovici dolžine paličastega preizkušanca (pri temperaturi, ki je mnogo nad tisto, uporabljeno pri preizkusih Gleeble)

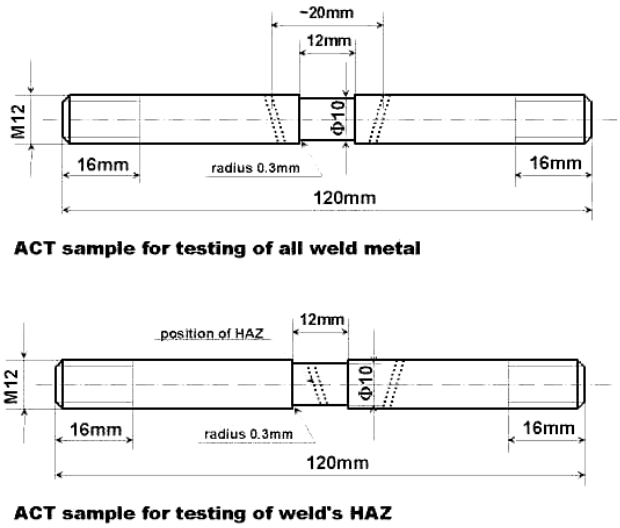

Figure 2: Cross-weld samples used for ACT on all-weld-metal and on weld's HAZ in the "SmartWeld" EU project

Slika 2: Preizkušanci z zvarom uporabljeni pri ACT, ki obsegajo cel zvar in toplotno cono pri projektu EU "SmartWeld"

Table 1: Chemical compositions of P91 weld metals
Tabela 1: Kemična sestava zvarov P91

Material	Element, *w*/%										
	C	Mn	Si	Cr	Ni	Mo	Nb	V	Ti	W	N
5s & 8s	0.06	0.59	0.36	9.49	0.94	0.98	0.005	0.21	0.000	0.21	
6s	0.06	0.60	0.37	9.12	0.90	0.97	0.005	0.20	0.000	0.20	
10s	0.09	0.84	0.40	8.70	0.40	0.93	0.061	0.21	0.008	0.01	+

$$F_{ACT} = P_{ACT} \cdot R_S / 100$$

where R_S is the average stress of all ACT cycles measured during relaxation on tension.

Selected examples of strain-time and stress-time graphs from ACT are in **Figures 3 to 6**; in the "soft", e.g. over-tempered material like sample 6s, the zero-stress line on the strain-time curve resembles well a normal creep graph with its three characteristic stages, see **Figure 3**, while for the "hard" materials like as-welded sample 5s and 10s, a straight continuous elongation in each cycle was observed from beginning till the end of test, **Figure 5**.

Selected examples of the ACT results on P91 weld metals are given in **Table 2** below. They show in general higher creep strength of non heat-treated weld metals, with tendency of increasing time to fracture by PWHT due to changing of failure micromechanism (compare 5s with 6s). They also show positive results of optimizing heat treatment (6s vs. 8s) as well as of the improved chemical composition (5s vs. 10s).

Table 2: Examples of ACT results
Tabela 2: Primeri ACT-rezultatov

Sample number	Material & state	ACT temp. °C	ACT time to fracture ks	Tensile relax stress R_S/MPa	Creep strength factor F_{ACT}/ MPa
5s	P91-AW	600	28.3	325	240
6s	P91-HT	620	45.2	177	137
8s	P91-HT	600	26.3	318	233
10s	P91-AW	600	82.6	336	262

In parallel, short-term creep-rupture tests (STCT) were run on these materials and the results of both tests compared. Selected results of the STCT are given in Table 3 and compared with those of the ACT. The creep strength factor – F_{CS} – given in this table was calculated from the STCT results like:

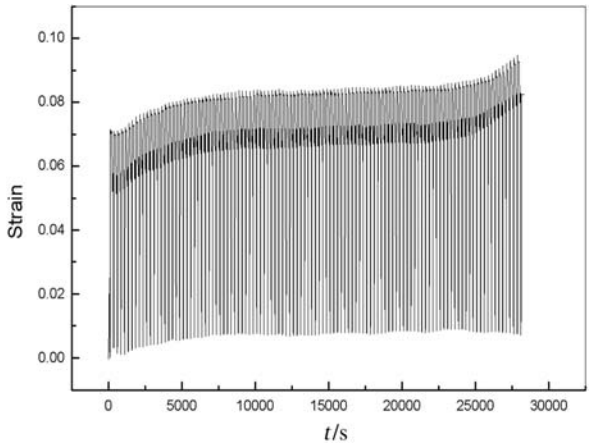

Figure 3: Typical strain-time graph from ACT on a "soft" weld metal – sample 6s
Slika 3: Značilna odvisnost deformacija-čas za ACT mehkega materiala zvara – vzorec 6s

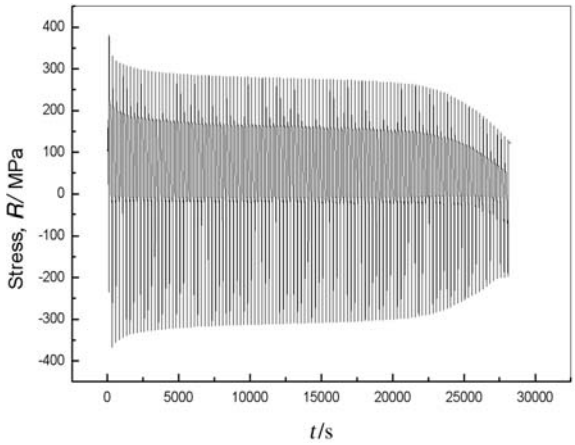

Figure 4: Typical stress-time graph from ACT on a "soft" weld metal – sample 6s
Slika 4: Značilna odvisnost napetost-čas za ACT mehkega materiala zvara – vzorec 6s

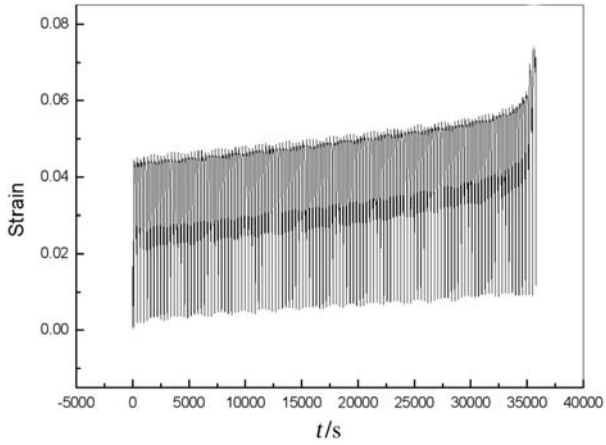

Figure 5: Typical strain-time graph from ACT on a "hard" weld metal – sample 5s
Slika 5: Značilna odvisnost deformacija-čas za ACT trdega materiala zvara – vzorec 5s

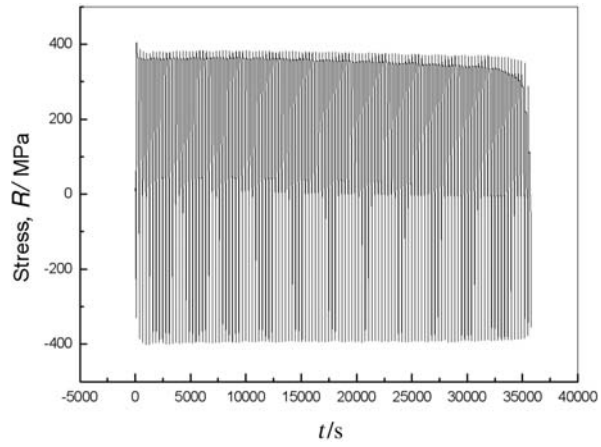

Figure 6: Typical stress-time graph from ACT on a "hard" weld metal – sample 5s
Slika 6: Značilna odvisnost napetost-čas za ACT trdega materiala zvara – vzorec 5s

Table 3: Comparison of results: ACT vs. STCT
Tabela 3: Primerjava rezultatov ACT in STCT

Sample No.	Material & state	STCT results: [temp/stress/time]	F_{CS}/MPa	F_{ACT}/MPa	F_{CS}/F_{ACT}
5s	P91-AW	620/130/381	262	240	1.09
6s	P91-HT	620/130/27	248	137	1.82
8s	P91-HT	620/130/31	249	233	1.07

$$F_{CS} = P_{LM} \cdot R_L/100$$

Where R_L is the initial stress of the constant-load short-term creep experiment and P_{LM} is the Larson-Miller parameter: $P_{LM} = (20 + \lg t) \cdot T/100$, with T = testing temp. in K and t = time to rupture in h.

3 INITIAL MICROSTRUCTURES

3.1 As welded samples 5s and 10s

The main component of the microstructure is acicular low-carbon martensite with high density of tangled dislocations (**Figures 7–10**). In this martensite numerous spheroidal inclusions of sub-micron size are present. In sample 5s fine cementite and very fine MX particles interact with dislocations, **Figure 8**. In sample 10s, in the inter-bead heat-affected zones along grain boundaries of former austenite, chains of middle-sized $M_{23}C_6$ carbides appear, **Figure 9**. In the columnar grain regions of very high dislocation density in sample 10s, (**Figure 10**), hexagonal M_2X particles as well as MX particles were identified. This martensitic microstructure should be considered as auto-tempered or tempered due to welding cycles, more in sample 10s than in 5s.

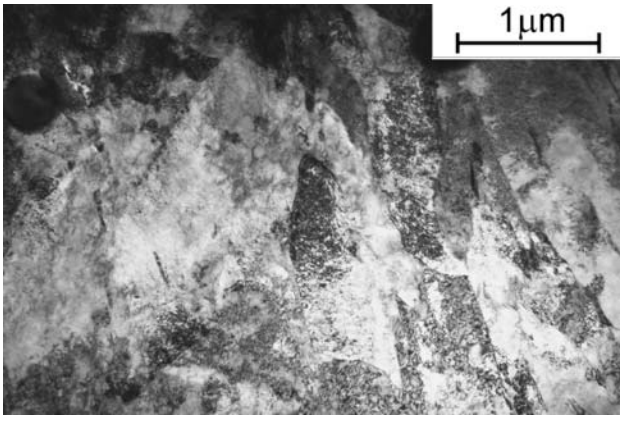

Figure 7: Acicular low-carbon martensite in as-welded sample 5s
Slika 7: Acikularni malooglјični martenzit v vzorcu zvara 5s

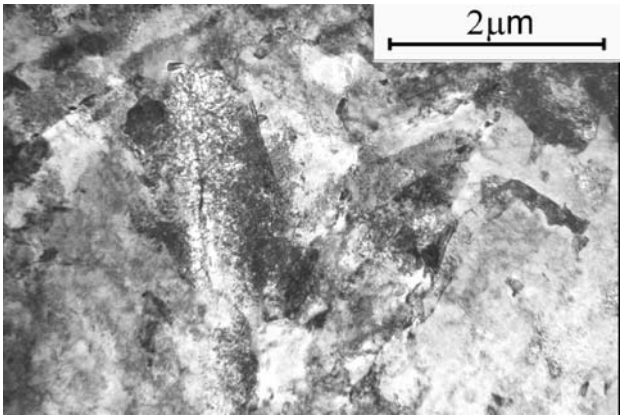

Figure 9: Carbides on former austenite grain boundaries in as-welded sample 10s
Slika 9: Karbidi na avstenitnih mejah v vzorcu zvara 10s

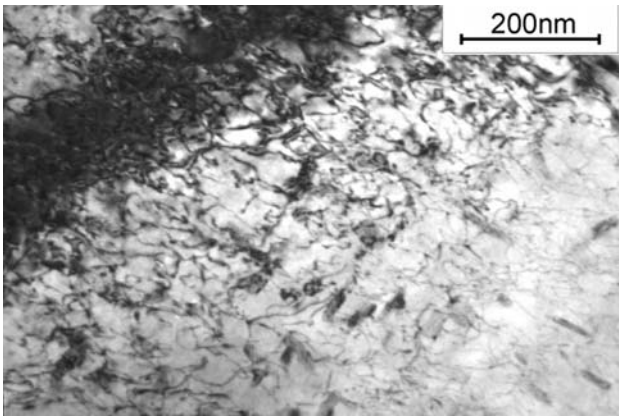

Figure 8: Cementite precipitated on dislocation tangles in as-welded sample 5s
Slika 8: Izločki cementita na vozliščih dislokacij v vzorcu zvara5 s

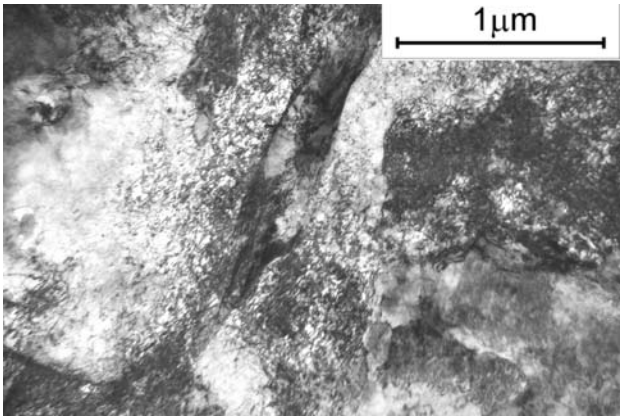

Figure 10: High density of dislocations in martensite of as-welded sample 10s
Slika 10: Velika gostota dislokacij v martenzitu v vzorcu zvara 10s

3.2 Post-weld heat-treated samples 6s and 8s

The post-weld heat-treated samples 6s and 8s had a tempered martensite microstructure with numerous subgrains, often retaining orientation of the former martensite laths (**Figures 11–13**). In both 6s and 8s samples, the former austenite grain boundaries as well as the post-martensitic lath boundaries were marked with coagulated $M_{23}C_6$ carbides. A very high dislocation density appeared in grains and subgrains of the inter-bead heat affected zones in sample 8s where also spheroidal carbides were present (**Figure 14**), while the overall microstructure of the sample 6s was much better recovered i.e. the dislocation density in it was visibly lower (**Figure 12**).

4 DEVELOPMENT OF MICROSTRUCTURE DURING ACT

Most of the accelerated creep tests were carried out up to appearance of fracture, in order to gain the date representative to the creep life of the materials.

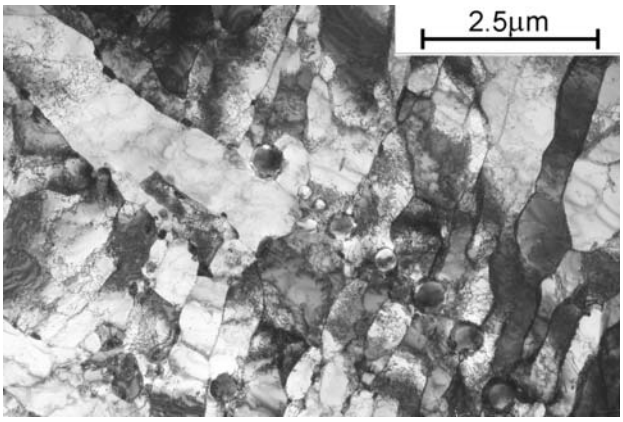

Figure 11: Arrays of ferrite subgrains and elongated grains in tempered sample 6s
Slika 11: Mreža podrzrn ferita in podolgovata zrna v popuščenem vzorcu 6s

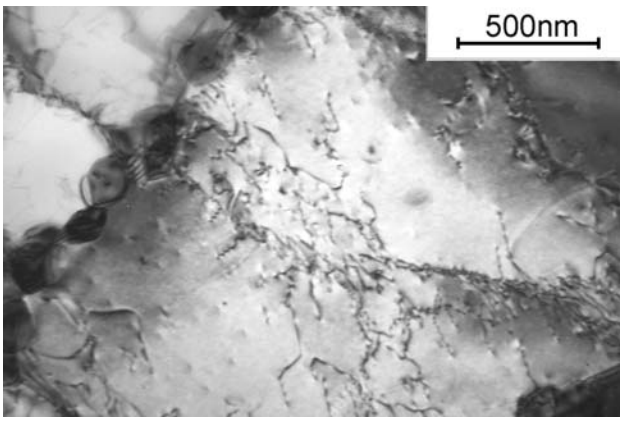

Figure 12: Chain of carbides along grain / subgrain boundary in sample 6s
Slika 12: Niz karbidov na meji zrno-podzrno v vzorcu 6s

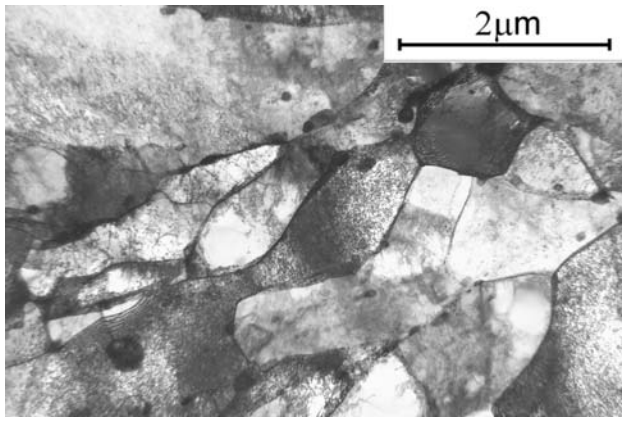

Figure 13: Fine ferrite grains/subgrains with high dislocation density in sample 8s
Slika 13: Majhna zrna/podzrna ferita v vzorcu 8s

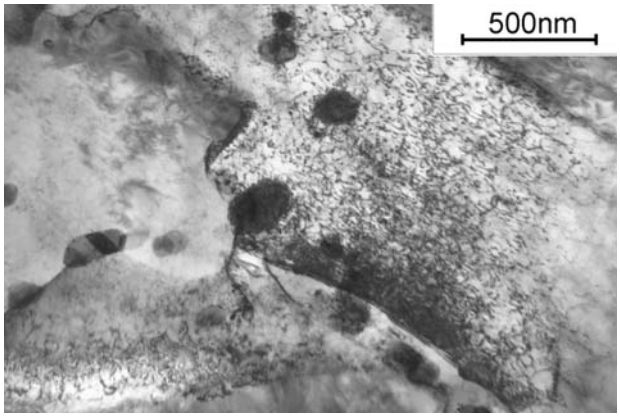

Figure 14: Spheroidal carbides in ferrite in the sample 8s
Slika 14: Sferoidirani karbidi v feritu v vzorcu 8s

Nevertheless, for the purpose of this study on the sequence of precipitation processes and changes in the weld metal matrix, several tests were interrupted and microstructure of the partly transformed samples examined.

4.1 ACT of sample 5s

The accelerated creep test of the as-welded sample results in transformation of the matrix and stimulates precipitation of carbides. Semi-recovered subgrains sized about 1–2 μm form in the matrix before the sample reaches 50 % of its life time in ACT (**Figure 15**). By this stage also the coalescence of subgrains begins, causing oriented chains of carbides to appear within the grains (**Figure 16**). By 80 % of the ACT duration the recrystallising ferrite grains reach 5 μm or more due to the coalescence of finer subgrains (**Figure 17**). At this stage, well-pronounced agglomerates of coagulated carbides can be observed along the former austenite grain boundaries, in particular near to the "triple points" (**Figure 18**). These carbides were mainly of $M_{23}C_6$ type, although some M_6C carbides could be identified as well.

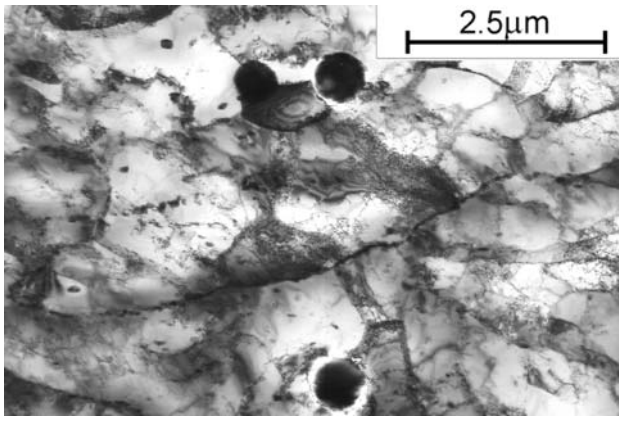

Figure 15: Formation of subgrains in sample 5s at half-life in ACT
Slika 15: Nastanek podrzrn pri polovici trajnostne dobe vzorca 5s v ACT

The finest precipitates dominating within the recovered post-martensitic subgrains, were positively identified as of cubic MX type, while some larger and elongated appeared to be of hexagonal M_2X type. On thin foil specimens, taken from near to fracture after completion of the ACT and examined in TEM, still some of these fine precipitates could be seen within the recrystallised ferrite grains.

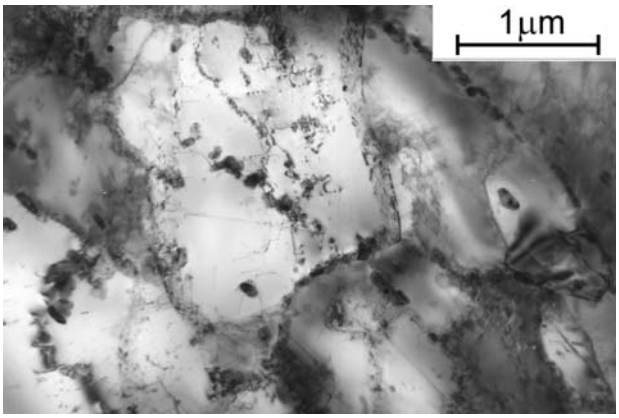

Figure 16: Chain of carbides inside growing subgrain in sample 5s
Slika 16: Nizi karbidov v rastočih podzrnih v vzrocu 5s

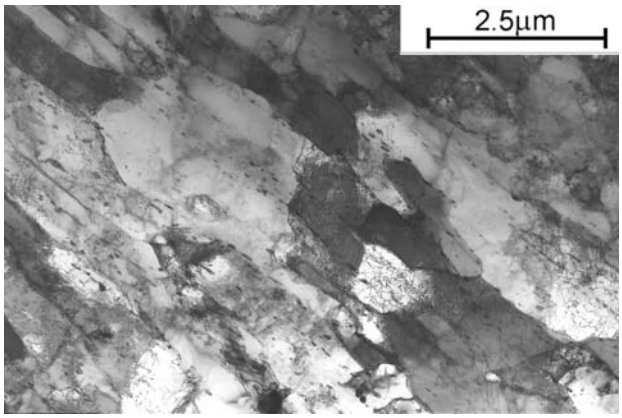

Figure 17: Incipient coalescence of subgrains in sample 5s at 80 % of life in ACT
Slika 17: Začetek koalaescence podzrn v vzorcu 5s pri 80 % trajnostne dobe v ACT

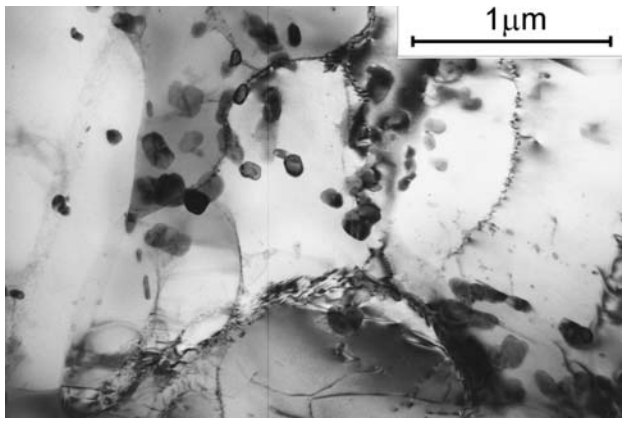

Figure 18: Agglomerate of carbides in the sample 5s at 80 % of life in ACT
Slika 18: Aglomerat karbidov v vzorcu 5s pri 80 % trajnostne dobe v ACT

4.2 ACT of samples 6s and 8s

In the over-tempered sample 6s, having already a well-recovered ferrite matrix with low dislocation density before the ACT, the ACT resulted in a fast recrystallisation of the matrix by coalescence of subgrains and coagulation of $M_{23}C_6$ carbides (**Figures 19 and 20**). The fine precipitates of MX carbo-nitrides disappeared almost entirely and the fine acicular M_2X phase also could not be found. Some larger precipitates appearing after completion of the ACT were identified as Laves phase.

The sample 8s having an initially less transformed matrix than 6s, with a high dislocation density, around the half of its life in the ACT showed substantial recovery of the dislocation substructure and intensive precipitation of mainly MX phase on the dislocations (**Figures 21 and 22**). This situation persisted till 80 % of

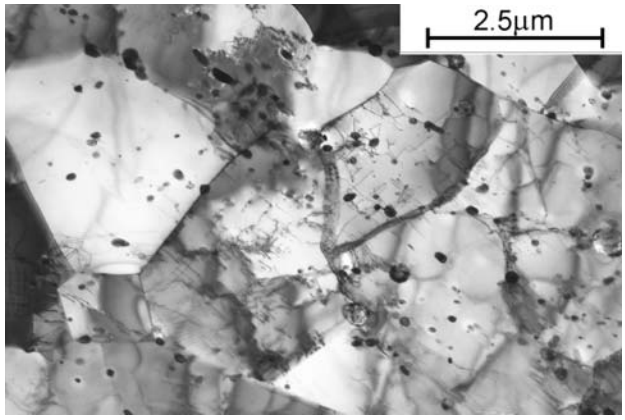

Figure 19: Fine recrystallised ferrite grains after ACT in sample 6s
Slika 19: Drobna rekristalizirana zrna ferita v vzorcu 6s po ACT

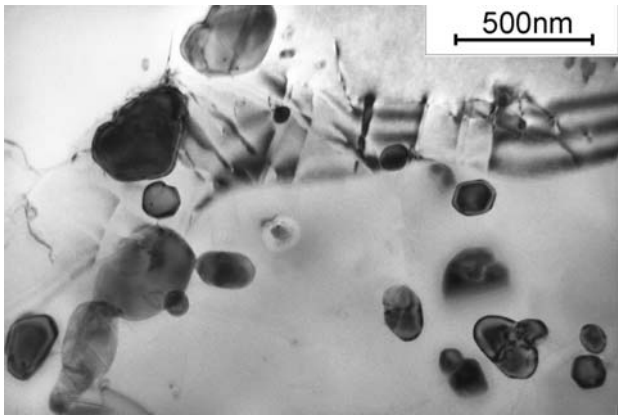

Figure 20: Spheroidised carbides after ACT in sample 6s
Slika 20: Sferoidizirani karbidi v vzorcu 6s po ACT

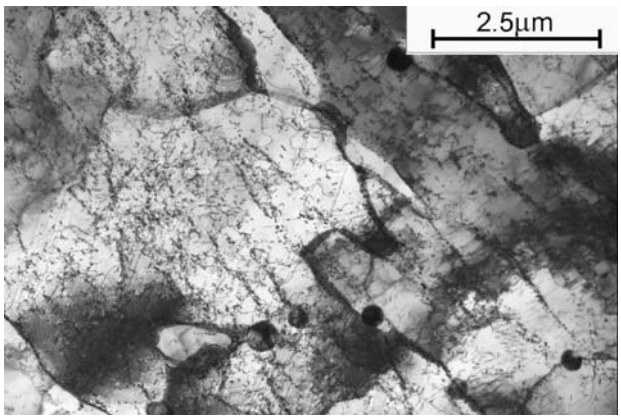

Figure 21: Subgrains with medium–density dislocations in sample 8s at half-life in ACT
Slika 21: Podzrno s srednjo gostoto dislokacij v vzorcu 8s po polovici ACT trajnostne dobe

the ACT duration, when visible coarsening of fine precipitates within subgrains occurred and more coagulated carbides of $M_{23}C_6$ and M_6C appeared on subgrain boundaries, as well as coalescence of subgrains progressed. Further on, till fracturing of the ACT sample, the fine precipitates within ferrite grains still

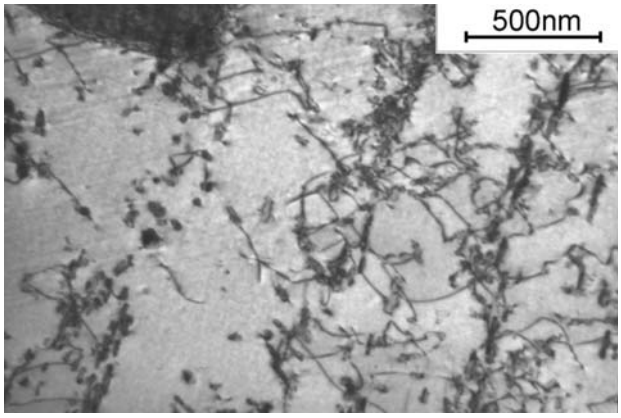

Figure 22: MX precipitates on dislocations in sample 8s
Slika 22: Izločki MX na dislokacijah v vzorcu 8s

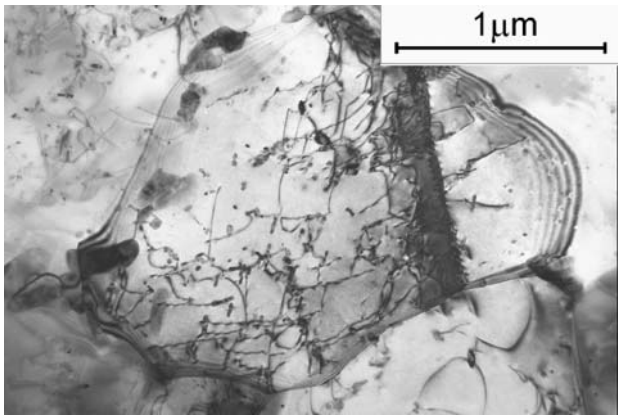

Figure 23: Recrystallised small grain with a few fine precipitates after ACT; sample 8s
Slika 23: Majhno rekristalizirano zrno s majhnimi izločki po ACT, vzorec 8s

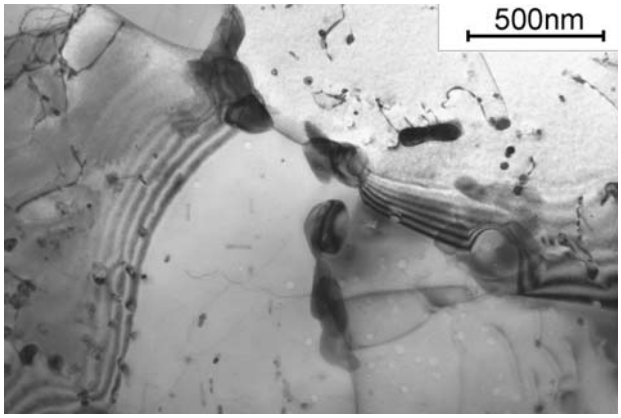

Figure 24: Agglomerate of platelike carbides at grain boundary after ACT; sample 5s
Slika 24: Aglomerat ploščatih karbidov na kristalni meji po ACT

existed (**Figure 23**), interacting with dislocations as well as pinning ferrite grain boundaries (**Figure 24**). Agglomerates of larger precipitates consisted mainly of $M_{23}C_6$ and M_6C, and minor amounts of Laves phase particles were associated with them.

4.3 ACT of sample 10s

The as-welded initial microstructure of sample 10s contained already the $M_{23}C_6$ carbides along prior austenite boundaries and MX plus M_2X phases within martensite laths before ACT. In the first half of the ACT duration the $M_{23}C_6$ carbides grew while the fine MX and M_2X prevented the dislocation recovery within subgrains (**Figures 25 and 26**). Around 80 % of the ACT life, mixed substructure dominated consisting of small recrystallised grains co-existed with non-recovered and well-recovered subgrains. By the end of ACT, the recrystallised ferrite grains (**Figure 27**), still co-existed with the subgrains, in which fine precipitates interacted with the medium-density configurations of recovered dislocations (**Figure 28**).

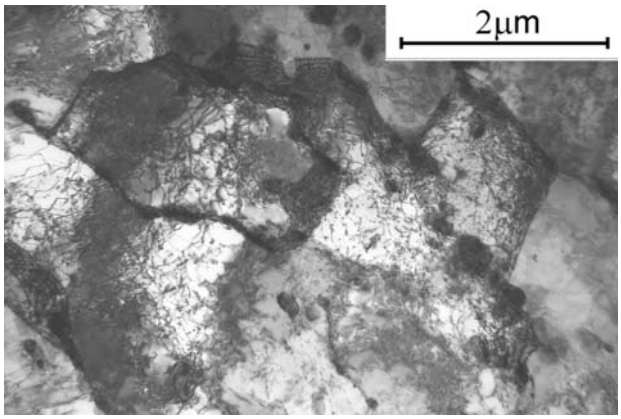

Figure 25: Subgrains with high dislocation density at half-life in ACT; sample 10s
Slika 25: Podzrno z visoko gostoto dislokacij v vzorcu 10s pri polovici ACT trajnostne dobe

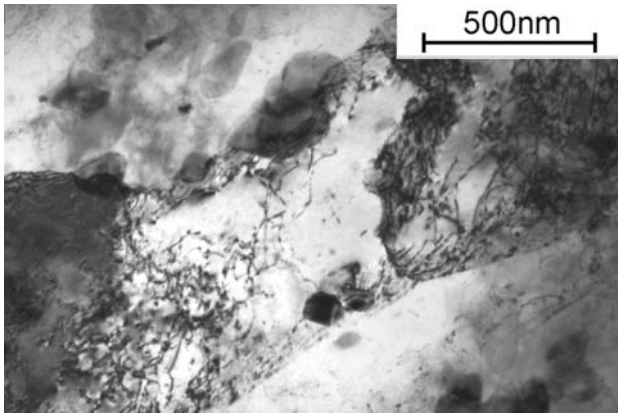

Figure 26: Precipitated coagulated carbides in sample 10s
Slika 26: Izločeni koagulirani karbidi v vzorcu 10 s

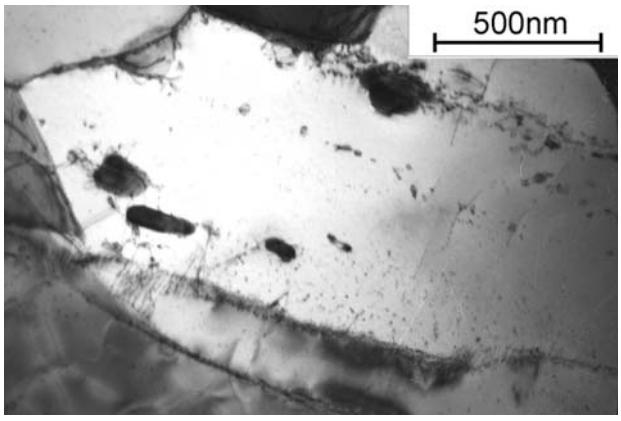

Figure 27: Small recrystallised ferrite grain with precipitates after ACT in sample 10s
Slika 27: Majhno rekristalizirano zrno z izločki po ACT vzorca 10s

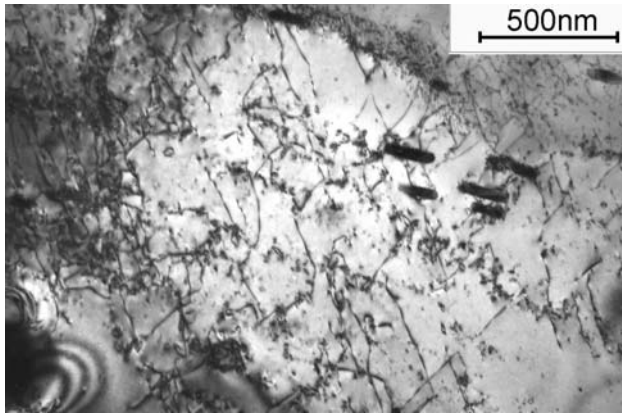

Figure 28: Recovered dislocations after ACT interacting with fine carbides; sample 10s
Slika 28: Dislokacije po popravi, ki reagirajo s drobnimi karbidi po ACT v vzorcu 10s

5 DISCUSSION

The results of this work show the behaviour of some P91 grade weld metals during accelerated creep tests. They allow comparing the standard / lean as-welded material 5s with the optimized one 10s, as well as evaluate the influence of heat treatment on the creep strength on the example of samples 6s and 8s.

Characteristic of the optimized weld metal 10s in its initial state were tortuous prior austenite grain boundaries in the inter-bead heat affected zones (**Figure 29**). This element of the microstructure was retained during the ACT and after completion of the test the precipitated carbides formed a pattern along the meandering grain boundaries (**Figure 30**). This might have been one of major factors responsible for the enhanced creep strength of the sample 10s in ACT and for its long creep life. In the case of the post-weld heat-treated weld metals 6s and 8s, evidently the heat treatment reduces the elevated temperature strength and for the samples tested by ACT in the simulated creep conditions this meants reduction of the creep strength and creep life. The accelerated creep test evidently causes further transformation of the microstructure and

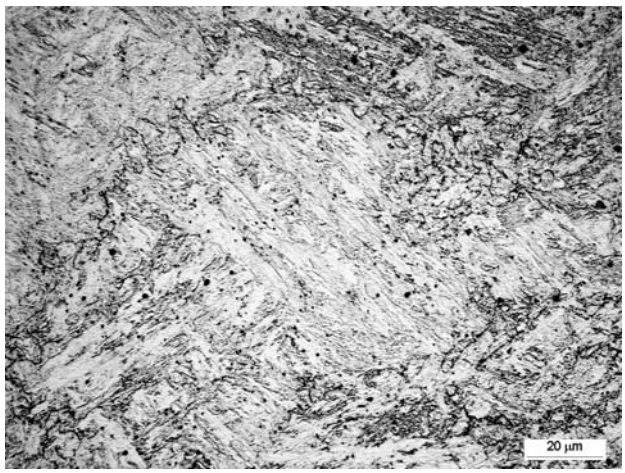

Figure 29: Tortuous prior austenite grain boundaries in as-welded sample 10s
Slika 29: Vijugasta meja avstenitnega zrna v zvaru vzorca 10 s

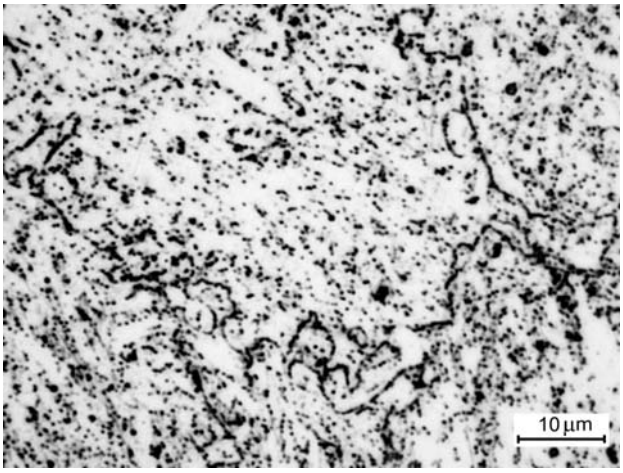

Figure 30: Meandering pattern of carbides precipitated after ACT in sample 10s
Slika 30: Meandraste oblike karbidov, ki so se izločili po ACT v vzorcu 10s

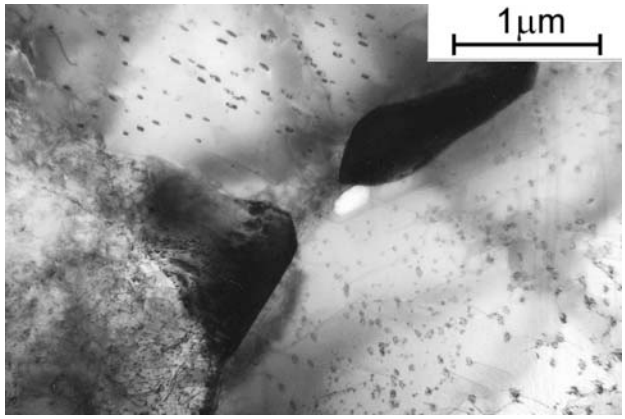

Figure 31: Fine MX precipitates in crept for 18 years 1.5Cr-1Mo-0.25V steel
Slika 31: Drobni MX-izločki v jeklu z 1.5Cr-1Mo-0.25V, ki je bilo 18 let izpostavljeno lezenju

enhances the precipitation. The question to be answered is whether all the ACT samples fail at the adequate transformation of the microstructure, similar to that of the real creep and are comparable with the results of other creep tests.

The results of EDS x-ray microanalysis are summarized in Table 4 below, together with Thermocalc data. Here (L) indicates the Laves phase present only in a part of the temperature range, while (Z) probably the z-phase not confirmed by diffraction. Then (x) refers to precipitates found on carbon extraction replica taken from ACT fracture while [x] the phases identified by SAD in thin foil specimens in TEM.

This table shows quite good correlation of ACT results with Thermocalc, except for the M_7C_3 presence on the replicas taken from the ACT fracture of the 8s sample. However, this non-equilibrium carbide may form when vast amount of dislocations annihilates, like during the recrystallisation after cold drawing of the 10Cr-2Si-Mo steel [2]. In fact, the ACT procedure uses a similar phenomenon of generating dislocations, allowing them to "inhale" interstitials and delivering the interstitials to the sites where dislocations annihilate.

Another question is due to the difference shown in Table 3 between ACT and STCT results on sample 6s, considered as over-tempered. In this sample from the beginning till the end of the ACT the finely-dispersed MX phase was almost absent. The MX is considered as an important creep strengthener, stable up to above 700 °C, interacting with dislocations and grain boundaries in steels exposed to creep [7]. Thus, in a 1.5Cr-1Mo-0.25V grade steel after exposure to creep for 18 years the MX is still present in most of ferrite grains (**Figure 31**). In the STCT tests of this research, the fine MX phase particles were only found in the as-welded material 5s, in minor amount of subgrains on thin foils taken from near to grip portions of the samples. Their traces could also be found in gauge portion of 8s STCT sample (**Figure 32**), but entirely not in the neck portion of 5s STCT

Table 4: Phase compositions of selected P91 weld metals (EDS microanalysis from carbon extraction replicas)
Tabela 4: Fazna sestava izbranih P91-zvarov (EDS-analiza na ogljikovih ekstrakcijskih replikah)

Sample & treatment	Accelerated creep test conditions	Phase composition / carbides						
		M_3C	$M_{23}C_6$	M_7C_3	M_2X	M_6C	MX	Laves etc.
5s – AW MMA, P91	Initial state	[x]	x				x	
	STCT – 620 °C/130/381h		x			x	x	
	ACT – 600 °C/26.6 ks		x			x	x	
8s – HT MMA, P91	STCT – 620 °C /130/31h		x				x	
	ACT – 600 °C/24.5 ks		x	(x)		x	x	L
5s & 8s	Thermocalc phase content at 500–620 °C		**X**			**X**	**X**	**(L)**
10s – AW MMA, P91	Initial state		x		x		x	
	ACT – 600 °C/82.6 ks		x			[x]	x	(Z)
10s	Thermocalc phase content at 500–620 °C		**X**			**X**	**X**	

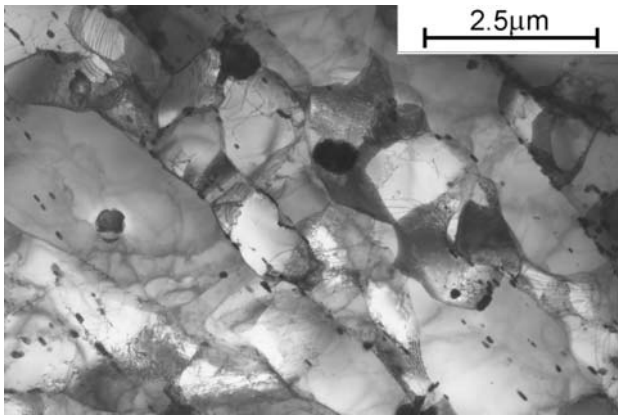

Figure 32: Subgrains and few fine carbides in gauge portion of 8s sample after STCT
Slika 32: Podzrna in drobni karbidi v merilni dolžini vzorca 8s po STCT

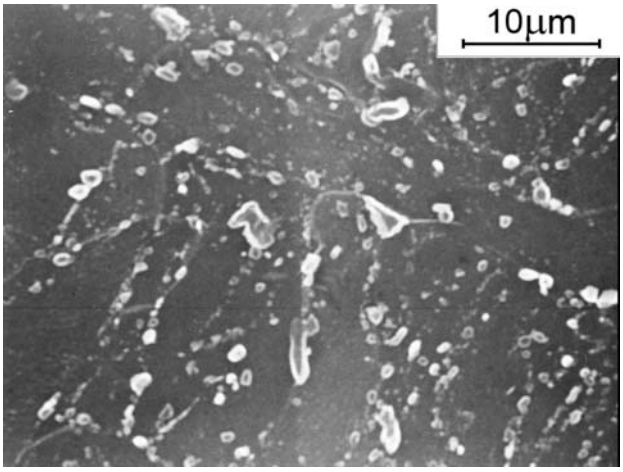

Figure 33: Different size carbides in crept for 9 years P91 weld metal; sample 1344/3
Slika 33: Karbidi različne velikosti v zvaru jekla P91, ki je bil izpostavljen lezenju 9 let, vzorec 1344/3

sample, where refinement of ferrite grains dominated certainly resulting from localized substantial strain. This grain refinement in the neck portion of the STCT samples was also characteristic of samples 6s and 8s.

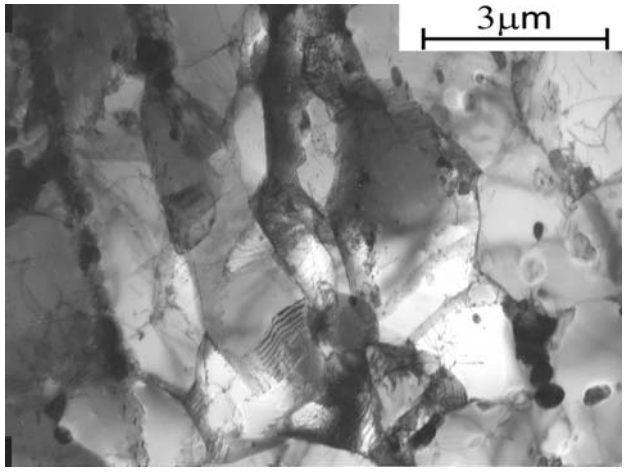

Figure 34: Elongated grains and subgrains of ferrite in crept sample 1344/3
Slika 34: Podolgovata zrna in podzrna ferita v vzorcu 1344/3, ki je bilo izpostavljen lezenju

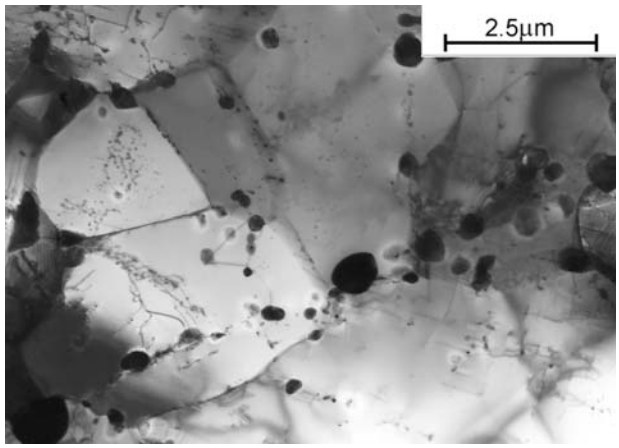

Figure 35: Recrystallised ferrite grains with coagulated $M_{23}C_6$ carbides; sample 1344/3
Slika 35: Rekristalizirano zrno ferita s koaguliranimi karbidi, vzorec 1344/3

As in this research the long-term creep tests were not carried out, a comparison is made here with the P91

Table 5: Chemical compositions of reference P91 weld
Tabela 5: Kemična sestava referenčnega zvara P91

Sample	Element, *w*/%									
	C	Mn	Si	Cr	Ni	Mo	V	Ti	Nb	**N**
KA 1344/3/ weld	0.10	0.42	0.28	8.01	0.14	0.92	0.21	0.00	0.060	0.045

Table 6: Phase compositions of reference P91 weld
Tabela 6: Fazna sestava referenčnega zvara P91

Sample	Creep conditions	Phase composition / carbides						
		M_3C	$M_{23}C_6$	M_7C_3	M_2X	M_6C	MX	Laves
KA1344/3 weld	Exploited ≈600 °C/ 170 bar/9 years		x				x	L
KA1344/3	Thermocalc phase content at 550–640 °C		X				X	L

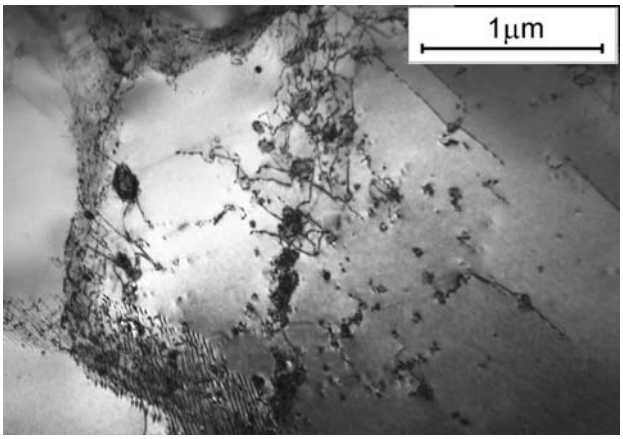

Figure 36: Fine MX precipitates interacting with dislocations in sample 1344/3
Slika 36: Drobni MX-izločki, ki reagirajo z dislokacijami v vzorcu 1344/3

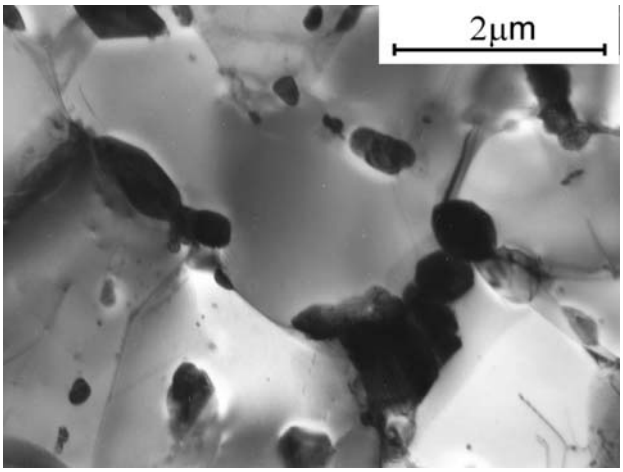

Figure 37: Agglomerates of $M_{23}C_6$ carbides in recrystallised matrix of sample 1344/3
Slika 37: Agmomerati $M_{23}C_6$-karbidov v rekristalizirani matici v vzorcu 1344/3

grade weld metal of a power plant component, marked KA 1344/3, which failed after exposure to creep at ≈600 °C/170 bar/9 years. The chemical composition of this reference weld is given in the **Table 5**, while the results of the phase identification are summarized in the **Table 6**.

Microstructure of this reference weld after 9 years exposure to creep, consisted of post-martensitic / ferritic matrix with precipitated phases of various sizes, some very large (**Figure 33**). A closer look into this microstructure by means of TEM on thin foil specimens, revealed the presence of numerous fine grains / subgrains retaining the post-martensitic orientation (**Figure 34**), as well as recrystallised equiaxial ferrite grains (**Figure 35**), with usually random distribution of carbides.

In numerous fine grains and subgrains some very fine MX precipitates were found interacting with dislocations

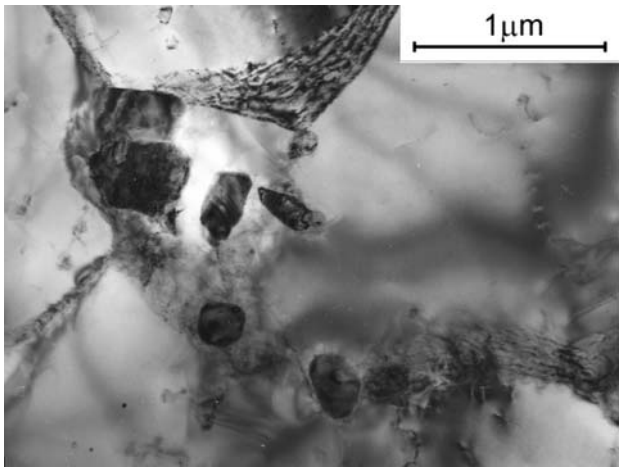

Figure 38: Medium size MX and $M_{23}C_6$ precipitates in sample 1344/3
Slika 38: Srednjeveliki izločki MX in $M_{23}C_6$ v vzorcu 1344/3

and low-angle boundaries (**Figure 36**). On former austenite grain boundaries and in the intersecting regions of former martensite laths, colonies of large carbides appeared, consisting of mainly $M_{23}C_6$ carbides and with a few MX precipitates (**Figure 37**). Other medium-size MX precipitates were found in the separate colonies, interacting with ferrite grain boundaries (**Figure 38**). The large $M_{23}C_6$ carbides often consisted of several crystallites separated by stacking faults and low angle boundaries (**Figures 39–40**). In several cases large M_6C carbides were identified, usually growing on the $M_{23}C_6$ carbides (**Figures 41 and 42**). Numerous of the large (>500 nm) $M_{23}C_6$ carbides possessed a substructure of "acicular type", which could be identified as a sandwich of stacking faults and/or very-thin (<10 nm) plate-like crystals (**Figures 43 and 44**). SAD patterns from such substructure exhibit double / multiple diffraction effects as well as reveal details of relative rotations between the

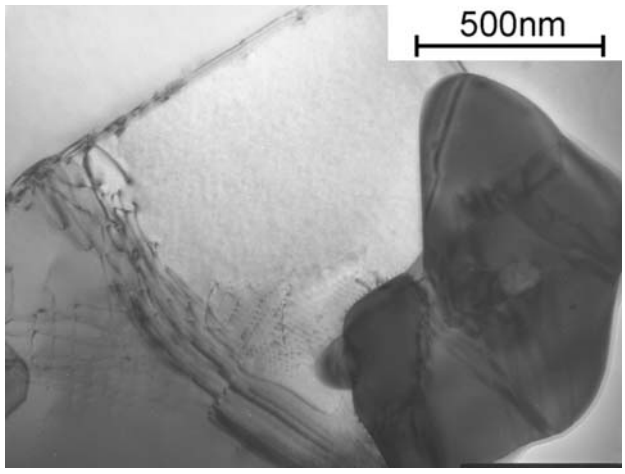

Figure 39: Large $M_{23}C_6$ carbide in recrystallised ferrite; sample 1344/3
Slika 39: Velik izloček karbida $M_{23}C_6$ v rekristsliranem feritu, vzorec 1344/3

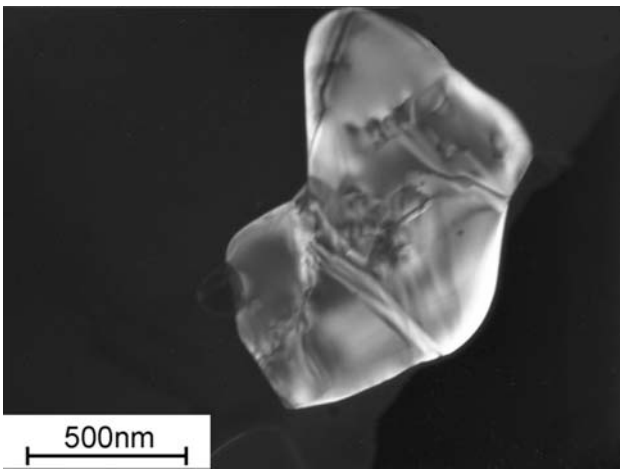

Figure 40: Dark field image of Figure 39: visible substructure / defects in the carbide
Slika 40: Karbid s slike 39 v temnem polju. Vidne so podstruktura in napake v karbidu

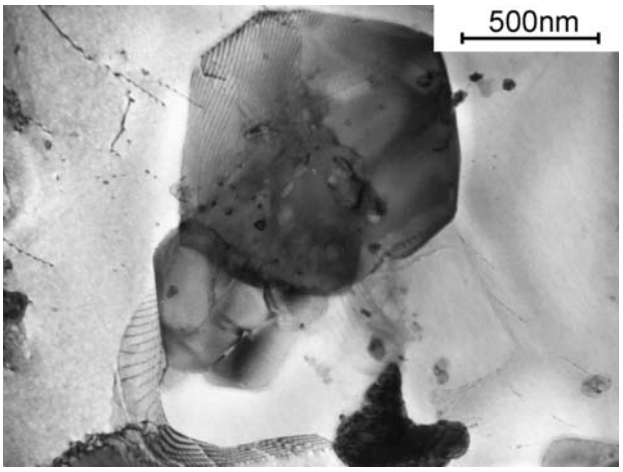

Figure 41: Large thin plate-like M_6C carbide overlapping with $M_{23}C_6$ carbide
Slika 41: Velik ploščat izloček karbida M_6C, ki se prekriva s karbidom $M_{23}C_6$

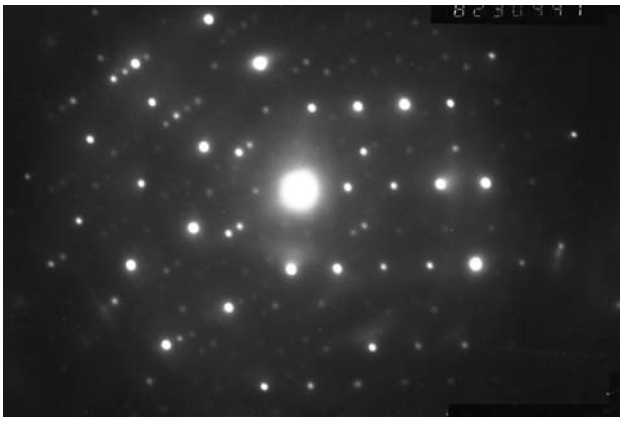

Figure 42: Diffraction from carbides of Figure 41, with double-diffraction effects
Slika 42: Difrakcija karbidov na sliki 41, dvojna difrakcijska slika

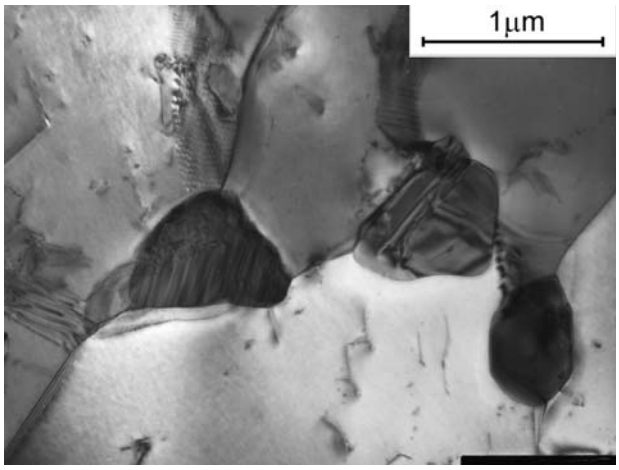

Figure 43: $M_{23}C_6$ carbides with stacking faults and fine plate-like substructure
Slika 43: Karbidi $M_{23}C_6$ z napakami zloga in fino ploščato podstrukturo

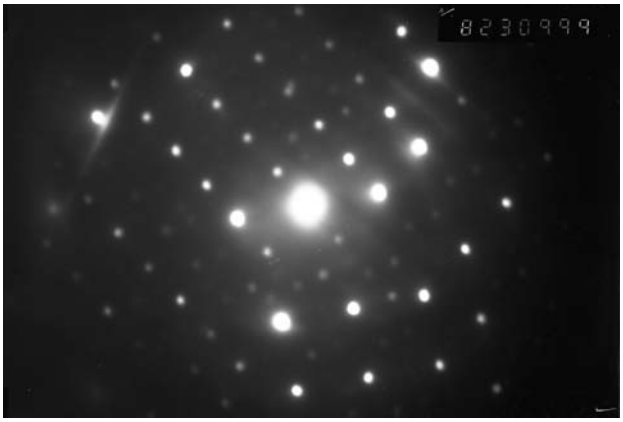

Figure 44: Diffraction from Figure 43, showing double-diffraction effects
Slika 44: Difrakcija s slike 43 z dvojnim difrakcijskim odsevom

platelets. In some cases Laves phase Fe_2Mo was identified as appearing in the sandwich structure.

In general, in the reference material 1344/3 the microstructure was inhomogeneous, which is typical for the weld metal. Accordingly, during creep it transformed non-uniformly, showing large precipitates next to completely recrystallised grains and some fine particles, mainly MX, interacting with dislocation and low angle boundaries in the regions where post-martensitic grains were retained.

As to the finely dispersed MX phase, which should support the creep strength, it was rather seldomly observed; more often the coagulated MX carbo-nitrides were present. It was recently suggested that the vanishing of the MX phase and decay of the creep strength might be due to formation of the Z-phase [8]. Although the observed features and chemical composition of the 1344/3 weld metal might have suggested that the Z-phase should appear in it, this phase was not

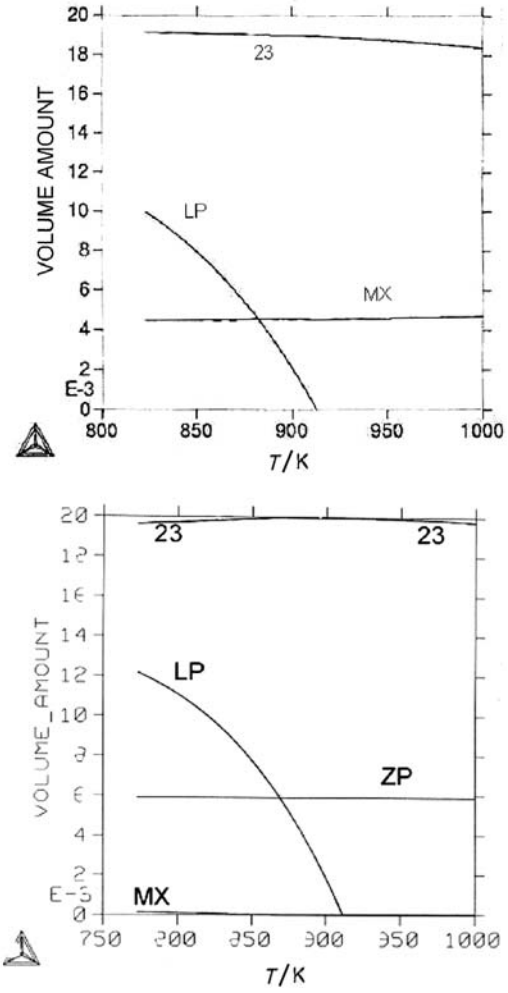

Figure 45: Thermocalc graphs for the reference P91 weld metal, for equilibrium state, without and with Z-phase (ZP); symbols: 23 = $M_{23}C_6$, LP = Laves phase

Slika 45: Thermocalc diagrami za referenčni var P91 za ravnotežno stanje brez in z Z-fazo; označbe: 23 = $M_{23}C_6$, LP = Lavesova faza

found in TEM/EDS investigation neither on carbon extraction replicas nor on thin foils.

From the above graphs (**Figure 45**) it is evident that when the Z-phase is present then the MX carbo-nitride disappears. Therefore the main question to be solved in further research is what caused the substantial decrease of the MX amount in the weld 1344/3, which had to be decommissioned prematurely due to the decrease of its high temperature strength. The lack of the Z-phase there might be explained by the failure occurring much before the phase equilibrium is reached. But this also confirms that the Z-phase was not here involved in the dissolution of the MX and decay of the properties. On the contrary, the Z-phase (or similar compound) appeared after ACT in the optimized P91 test weld metal 10s. However in this 10s material up to the failure of the ACT sample a large amount of the MX phase was still present.

6 CONCLUSIONS

1. The accelerated creep test on Gleeble (ACT) transforms microstructure of creep resisting weld metal in less than 50 hours similarly to that calculated by Thermocalc for phase equilibrium conditions.

2. The ACT gives results comparable with short-term creep tests (STCT), nevertheless microstructural investigations are helpful to explain differences if these occur.

7 REFERENCES

[1] Kidin I. N. Fizicheskie osnovy elektrotermicheskei obrabotki metallov i splavov; Izd. Metallurgia, Moscow 1969 (in Russian)

[2] Mandziej S., Marciniak J. TEM investigations on in-situ transformation of $M_{23}C_6$ carbides; Proc XIth Int Congr on Electron Microscopy, Kyoto 1986, 1271–72

[3] Mandziej S. T. Low-energy dislocations and ductility of ferritic steels; Materials Science & Engineering A, 164 (**1993**), 275–280

[4] Mandziej S. T., Výrostková A. Accelerated creep testing (ACT) procedure for weld metals using Gleeble systems, Gleeble Application Note, DSI, Poestenkill NY, USA, 2001

[5] Mandziej S. T., Výrostková A. Accelerated creep testing of P91 weld metals, IIW Doc II-1461–02.

[6] Pepe J. J., Gonyea D. C. Constant displacement rate testing at elevated temperatures in: Fossil Power Plant Rehabilitation, ASM International, Proc Int Conf, Cincinnati OH, Feb.1989, 39–45

[7] Woodhead J. H., Quarrell A. G. Role of carbides in low-alloy creep resisting steels; Journal of Iron and Steel Institute, (1965) June, 605–620

[8] Danielsen H. K. and Hald J. Behaviour of Z-phase in 9–12 % Cr steels, Energy Materials, 1 (**2006**) 1, 49–57